

Enhancing effectiveness of lubricated systems: Interplay of electrokinetics, hydrodynamics, substrate compliance and fluid rheology

Siddhartha Mukherjee¹, Sunando DasGupta^{1,2}, Suman Chakraborty^{1,3}

¹*Advanced Technology Development Center, Indian Institute of Technology Kharagpur, Kharagpur, India-721302*

²*Department of Chemical Engineering, Indian Institute of Technology Kharagpur, Kharagpur, India-721302*

³*Department of Mechanical Engineering, Indian Institute of Technology Kharagpur, Kharagpur, India-721302*

Enhancing the effectiveness of lubricated systems extensively used in research communities still remains a challenging proposition. In recent years, some efforts have been made in coupling interfacial phenomenon like electrokinetics with lubricated systems for improved performance, but were relatively scarce. Towards this, employing an intricate coupling between substrate compliance, hydrodynamic and electrokinetic modulations we have analyzed the alteration in the flow physics in a deformable microchannel under the rheological premises of viscoelastic fluids which closely resemble bio-fluids typically used in several bio and micro-fluidic applications. Here, we show that by making a judicious combination of involving parameters like concentration and molecular weight of polymer, concentration of electrolyte, monitoring the quality of Newtonian solvent one can achieve substantial augmentation in the load carrying capacity of the microchannel, thus having immense implications for novel design and performance of lubricated systems.

1 Introduction

Lubricated systems are omnipresent in the engineering settings as well as in the physiological systems.¹⁻¹⁸ The utilization of such systems has attracted significant attention in the research communities owing to their wide gamut of applications ranging from traditional engineering problems to biological processes. The performance of these systems is governed by their load bearing capacities which is a quantification of enduring maximum amount of load.^{5,6,19-24} A number of researches have been directed towards coupling interfacial phenomenon like electrokinetics with these systems in a vision to improve the performance.²⁵⁻³¹ One common feature of these systems is that they are often associated with flexible substrates thus making an interfacing between solid substrate and fluidic media, commonly termed as fluid-structure interaction (FSI).^{12,25,30,32-37} These systems are further characterized by wettability and surface charge modulations³⁸⁻⁴⁴ which are typically observed in narrow confinement flows interfacing with biological premises or may also be imposed by virtue of engineered approach.⁴⁵⁻⁴⁹

Recently, there is a propensity of utilizing complex non-Newtonian fluids in several micro and nanofluidic applications because of close similarities in their constitutive behaviour with biological fluids.⁵⁰⁻⁵⁴ Subsequently, constitutive relations have been proposed to describe the behaviour of biofluids, namely, power-law model,⁵⁵ Casson model,⁵⁶ Carreau model,^{57,58} (for inelastic fluids) and Maxwell model,^{54,59} Oldroyd-B model,⁶⁰ Phan-Thien Tanner model⁶¹⁻⁶⁶ (for viscoelastic fluids) to name a few. While a number of research works in FSI can be observed in the domain of in-vitro bio fluid mechanics, they are mainly restricted to delineating physiological aspects of FSI without considering the rheological complexity of bio-fluids.^{67,68} In this context, we have theoretically studied the deformation characteristics of a parallel plate microchannel subjected to the aforementioned modulations under the rheological premises of viscoelastic fluids. This analysis unveils that by making a suitable combination of experimentally tunable parameters like polymer concentration, polymer molecular weight, regulating the quality of Newtonian solvent and altering the electrolyte concentration, it is practically possible to augment the load bearing capacity of deformable microfluidic channel up to one order of magnitude with respect to Newtonian fluid. It is envisaged that, the outcomes of present analysis holds significant engineering as well as physiological relevance by constructing a new paradigm towards novel design and optimal performance of bio-mimetic lubricated devices.

2 Problem Formulation

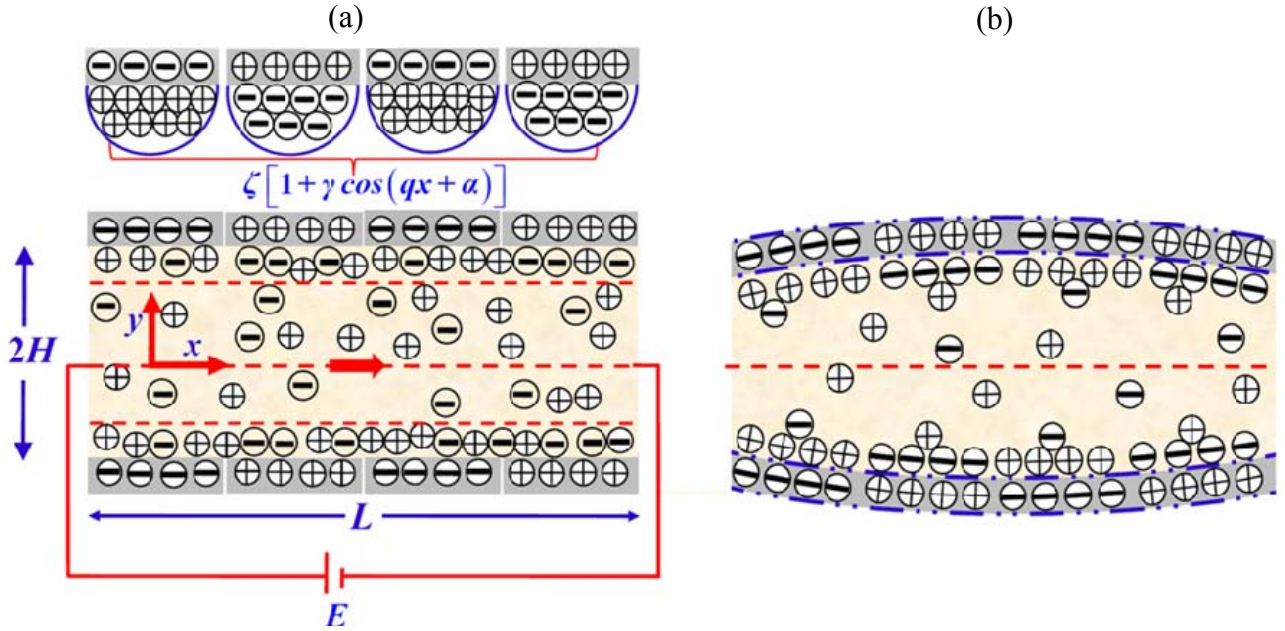


Fig. 1 Schematic of the electroosmotic flow in a parallel plate microchannel.(a) Un-deformed microchannel, (b) Deformed microchannel.

The physical domain of the present analysis consists of a parallel plate microchannel whose surfaces are compliant in nature. Rectangular Cartesian co-ordinate system has been chosen where x and y are the longitudinal and transverse co-ordinates with $y = 0$ being the origin of the physical domain. The length of the microchannel (l) is much higher as compared to the half channel height, (h) i.e., $l \gg h$. Here, the flow is actuated by means of an externally applied axial electric potential where a binary, symmetric (1:1) electrolyte solution is employed. The channel walls are subjected to axial modulations in the hydrodynamic slip length in association with the surface charge patterning, which take the following form $l_s [1 + \delta \cos(qx + \theta)]$ and $\zeta [1 + \gamma \cos(qx + \alpha)]$ ^{38,39,69–71} where l_s and ζ are the slip length and surface potentials, δ and γ are the axial modulations, q patterning frequency and θ (or α) being the phase difference between the axially varying and invariant components. In absence of any hydrodynamic and electrokinetic modulation, it represents the scenario of purely electroosmotic flow with uniform velocity profile and as a result, the presence of surface compliance has no effect. Any non-uniformity in the flow physics comes from the interaction between the modulation parameters which creates an imbalance in the pressure distribution. Now the

channel walls, because of its inherent compliant nature, try to maintain the original separation between them. This creates an axial pressure gradient and the associated lift force at the walls and the channel undergoes finite deformation. To obtain the extent of deformation, normal stress balance at the solid-fluid interface must be employed which reads ^{6,72,73}

$$\nabla \cdot \sigma = 0 \quad (1)$$

where $\sigma = \mathcal{G}(\nabla \vec{h} + \nabla \vec{h}^T) + \Lambda \nabla \cdot \vec{h} [I]$. For an isotropic, linearly elastic solid substrate, \mathcal{G} and Λ are the Lamé constants while $\vec{h} = [h_x, h_y]^T$ corresponds to the displacement field vector. One can simplify this equation using the assumption $l \gg h$ which leads to the following expression for the displacement field

$$\frac{\partial^2 h_y}{\partial y^2} = 0 \quad (2)$$

To solve this equation, one needs to incorporate the no-displacement condition at the compliant layer-solid interface (i.e. at $y = h$, $h_y = 0$) while normal stress balance prevails at the compliant layer-fluid interface (i.e. at $y = h - h_c$, $\sigma \cdot \hat{n} = -p \hat{n}$). This results in simplified form of h_y as

$$h_y = -\left(\frac{h_c}{2\mathcal{G} + \Lambda}\right)p \quad (3)$$

In equation (3), p is the hydrodynamic pressure. The compliant layer thickness is taken as h_c which correlates the stiffness factor of the channel as $\left(\frac{h_c}{2\mathcal{G} + \Lambda}\right) = S^{-1}$ where S represents the stiffness of the channel. Depending on the value of S , it may experience transition from the compliant regime to the stiff regime. For the transport phenomenon, the flow is assumed to be steady, laminar, and incompressible and in the creeping flow regime. The governing momentum and continuity equations are given below

$$\left. \begin{array}{l} \text{Continuity Equation :} \\ \text{Momentum Equations :} \end{array} \right\} \left[\begin{array}{l} \nabla \cdot \mathbf{v} = 0 \\ \begin{cases} x\text{-component :} & 0 = -\frac{\partial p}{\partial x} + \frac{\partial \tau_{xx}}{\partial x} + \frac{\partial \tau_{yx}}{\partial y} + \rho_e E_x \\ y\text{-component :} & 0 = -\frac{\partial p}{\partial y} + \frac{\partial \tau_{xy}}{\partial x} + \frac{\partial \tau_{yy}}{\partial y} + \rho_e E_y \end{cases} \end{array} \right] \quad (4)$$

where τ is the stress tensor, $E = -\nabla\phi$ induced electric field owing the application of the axial electric potential (ϕ), ρ_e excess charge density obtained from Poisson equation as $\nabla^2\phi = -\rho_e/\varepsilon$ with ε being the permittivity of the medium. There is an alteration in the chemical state of the surface when it comes into contact with an electrolyte solution, this results in acquiring some finite charge at the surface which is accompanied by the release of counter-ions to maintain electro-neutrality of the system. When an external potential is applied, although the system is electrically neutral overall, it possesses a net charge which drags the fluid in the axial direction and the electroosmotic flow is actuated. Here, a charged layer is formed in the close proximity of the solid substrate which consists of charge equal and opposite to the surface charge and this layer is known as Electrical double layer (EDL).⁷⁴⁻⁸⁰ With the weak electric-field approximation, ϕ can be represented as the linear superposition of two components, i.e., $\phi(x, y) = \phi_{ext}(x) + \psi(x, y)$ where $\phi_{ext}(x)$ is the externally applied potential with $\psi(x, y)$ being the potential induced within the EDL. With $l \gg h$, the charge distribution in the EDL gets simplified to the form of $d^2\psi/dy^2 = -\rho_e/\varepsilon$ (using $l \gg h$, $\partial\psi/\partial x \ll \partial\psi/\partial y$ and $d^2\phi_{ext}/dx^2 \ll d^2\psi/dy^2$). Further simplification is done by invoking the Debye-Hückel linearization approximation (valid for low surface potential, i.e. $\zeta < 25$ mV)^{39,69,81} which yields $\kappa^2\psi = -\rho_e/\varepsilon$ with κ being the inverse of the EDL thickness.

To describe the rheological behavior of the fluid, we have chosen the constitutive equation of the simplified Phan-Thien-Tanner model(sPTT).⁶¹⁻⁶³ For this model, the stress components take the following form^{65,82}

$$\begin{aligned}
F\tau_{xx} + \lambda \left(u \frac{\partial\tau_{xx}}{\partial x} + v \frac{\partial\tau_{xx}}{\partial y} - 2 \frac{\partial u}{\partial x} \tau_{xx} - 2 \frac{\partial u}{\partial y} \tau_{yx} \right) &= 2\mu \frac{\partial u}{\partial x} \\
F\tau_{yy} + \lambda \left(u \frac{\partial\tau_{yy}}{\partial x} + v \frac{\partial\tau_{yy}}{\partial y} - 2 \frac{\partial v}{\partial x} \tau_{xy} - 2 \frac{\partial v}{\partial y} \tau_{yy} \right) &= 2\mu \frac{\partial v}{\partial y} \\
F\tau_{xy} + \lambda \left(u \frac{\partial\tau_{xy}}{\partial x} + v \frac{\partial\tau_{xy}}{\partial y} - \frac{\partial u}{\partial y} \tau_{yy} - \frac{\partial v}{\partial x} \tau_{xx} \right) &= \mu \left(\frac{\partial u}{\partial y} + \frac{\partial v}{\partial x} \right)
\end{aligned} \tag{5}$$

where $\mu = \mu_p + \mu_s$ is the fluid viscosity consisting of both polymeric component (μ_p) as well as its Newtonian counterpart (μ_s) (i.e. solvent) and λ is the fluid relaxation time, a characteristic time scale of a viscoelastic fluid. Also, F is the stress coefficient for the stress tensor

$F = [1 + \epsilon \lambda \text{tr}(\boldsymbol{\tau}) / \mu]$ with ϵ being the fluid extensibility which in the limit of $\epsilon \rightarrow 0$ represents a simpler upper-convected Maxwell (UCM) model. Choosing proper scales for the stress components, one can simplify the stress components where a relationship between the tangential stress (τ_{xy}) and normal stress (τ_{xx}) can be established as $\tau_{xx} = 2\lambda \tau_{xy}^2 / \mu$.^{65,82} Using this relationship, one can simplify the flow field in the following manner

$$\frac{\partial u}{\partial y} = \frac{\tau_{xy}}{\mu} + \frac{2\epsilon \lambda^2}{\mu^3} \tau_{xy}^3 \quad (6)$$

The governing equations are now subjected to the modulated slip and zeta potential boundary conditions, as shown in the following

$$\left. \begin{aligned} u|_{y=\pm H} &= \mp l_s [1 + \delta \cos(qx + \theta)] \frac{\partial u}{\partial y} \Big|_{y=\pm H} \\ \text{and } \psi|_{y=\pm H} &= \zeta [1 + \gamma \cos(qx + \alpha)] \end{aligned} \right\} \quad (7)$$

The analytical approach for the solution procedure along with the solution is discussed in detail in the following section.

3 Analytical solution procedure

In order to take into account the combined effect of wettability and surface charge modulation, we expand any field variable in an asymptotic series in the following manner

$$\varphi = \varphi_0 + \delta(\varphi_{11}) + \gamma(\varphi_{12}) + \delta^2(\varphi_{21}) + \gamma^2(\varphi_{22}) + \delta\gamma(\varphi_{23}) \quad (8)$$

Using the asymptotic expansion of Eq. (8), the x -component of the momentum equation along with Eq. (6) are rewritten below

$$\left. \begin{aligned} 0 &= -\frac{d}{dx} \left(\begin{array}{c} p_0 + \delta p_{11} + \gamma p_{12} \\ + \delta^2 p_{21} + \delta \gamma p_{23} \end{array} \right) + \frac{\partial}{\partial y} \left(\begin{array}{c} \tau_{xy,0} + \delta \tau_{xy,11} + \gamma \tau_{xy,12} \\ + \delta^2 \tau_{xy,21} + \delta \gamma \tau_{xy,23} \end{array} \right) - \epsilon \kappa^2 (\psi_0 + \gamma \psi_{12}) E \\ \frac{\partial}{\partial y} \left(\begin{array}{c} u_0 + \delta u_{11} + \gamma u_{12} \\ + \delta^2 u_{21} + \delta \gamma u_{23} \end{array} \right) &= \frac{1}{\mu} \left(\begin{array}{c} \tau_{xy,0} + \delta \tau_{xy,11} + \gamma \tau_{xy,12} \\ + \delta^2 \tau_{xy,21} + \delta \gamma \tau_{xy,23} \end{array} \right) + \frac{2\epsilon \lambda^2}{\mu^3} \left(\begin{array}{c} \tau_{xy,0} + \delta \tau_{xy,11} + \gamma \tau_{xy,12} \\ + \delta^2 \tau_{xy,21} + \delta \gamma \tau_{xy,23} \end{array} \right)^3 \end{aligned} \right\} \quad (9)$$

One interesting thing to note that the potential distribution gets influenced only due to surface charge modulation (involving $O(\gamma^0)$ and $O(\gamma)$ terms) while the coupling between two perturbations are incorporated through $O(\delta\gamma)$ term. Similarly, the boundary conditions are also expanded as

$u_{hs} = -\varepsilon E\zeta/\mu$ (commonly known as Helmholtz-Smoluchowski velocity scale).

$$\left. \begin{aligned} 0 &= -\frac{dp_{11}}{dx} + \frac{\partial \tau_{xy,11}}{\partial y} \\ \frac{\partial u_{11}}{\partial y} &= \frac{\tau_{xy,11}}{\mu} + \frac{6 \in \lambda^2}{\mu^3} \tau_{xy,0}^2 \tau_{xy,11} \quad \text{where } \tau_{xy,11} = \frac{dp_{11}}{dx} y \end{aligned} \right\} \quad (14)$$

The corresponding velocity profile is given by

$$\left. \begin{aligned} u_{11} &= \frac{y^2 u_{hs}}{2} \frac{dp_{11}}{dx} + \frac{3}{2} \frac{sDe^2 u_{hs} \left(\frac{dp_{11}}{dx} \right)}{\kappa^2 \cosh^2(\kappa h)} \left\{ \kappa y \sinh(2\kappa y) \right\} - l_s u_{hs} \left\{ \frac{dp_{11}}{dx} h + 6sDe^2 h \tanh^2(\kappa h) \right\} \\ -l_s u_{hs} \cos(qx + \theta) &\left\{ \begin{aligned} & \left\{ \begin{aligned} & -\kappa \tanh(\kappa h) \\ & -2sDe^2 \kappa \tanh^3(\kappa h) \end{aligned} \right\} \\ & - \frac{h^2 u_{hs}}{2} \frac{dp_{11}}{dx} - \frac{3}{2} \frac{sDe^2 \left(\frac{dp_{11}}{dx} \right) u_{hs}}{\cosh^2(\kappa h) \kappa^2} \left\{ \begin{aligned} & \kappa h \sinh(2\kappa h) \\ & -\kappa^2 h^2 - \cosh^2(\kappa h) \end{aligned} \right\} \end{aligned} \right\} \end{aligned} \right\} \quad (15)$$

Unlike $O(1)$ solution, here channel height becomes axially variant $h(x)$ which takes into account the effect of surface compliance as $h(x) = h + d(x)$ where h is the axially invariant part and $d(x)$ is the deformation caused by any kind of perturbation which is determined from the stress balance at the solid-fluid interface as discussed earlier. Here, we represent the two-dimensional flow in terms of the classical Reynolds equation as ^{6,73}

$$\int_{-h}^h \frac{\partial u_{11}}{\partial x} dy + \int_{-h}^h \frac{\partial v_{11}}{\partial y} dy = 0 \quad (16)$$

where the v -component can be obtained by using no-penetration condition at the surfaces (i.e. $v|_{y=\pm h} = 0$). Further simplification of Eq. (16) can be done by applying Leibnitz's rule of differentiation under the integral which yields

$$\int_{-h}^h \frac{\partial u_{11}}{\partial x} dy = \frac{\partial}{\partial x} \int_{-h}^h u_{11} dy - u_{11}(y=h) \frac{\partial h}{\partial x} + u_{11}(y=-h) \frac{\partial(-h)}{\partial x} = 0 \quad (17)$$

Eq. (17) results in a differential equation describing the following pressure distribution in the axial direction where some mathematical simplifications are chosen like $\{h(x)\}^3 \approx h^3$, $\{h(x)\}^2 \approx h^2$ and $\tanh\{\kappa h(x)\} \approx \tanh(\kappa h)$

$$\chi_1 \frac{d^2 p_{11}}{dx^2} + \chi_2 \left(\frac{dp_{11}}{dx} \right)^2 + \chi_3 = 0 \quad (18)$$

Now, we non-dimensionalise all variables involved in Eq. (18) in the following way

$$\left. \begin{aligned} \bar{x} &= x/l, \bar{y} = \bar{h} = h/l, \bar{p} = (p - p_{atm})l/\mu u_{hs}, \bar{\kappa} = \kappa l, \\ \bar{q} &= ql, l_s = l_s/l, \bar{\psi} = \psi/\zeta, \beta = \mu u_{hs}/Sl^2 \end{aligned} \right\}$$

and the corresponding dimensionless form of Eq. (18) is written below

$$\bar{\chi}_1 \frac{d^2 \bar{p}_{11}}{d\bar{x}^2} + \bar{\chi}_2 \left(\frac{d\bar{p}_{11}}{d\bar{x}} \right)^2 + \bar{\chi}_3 = 0 \quad (19)$$

The coefficients involved in Eqs. (18)-(19) can be found in **Section E** of the supplementary material. Since Eq. (19) is inherently non-linear in nature, it becomes analytically intractable. Hence, one needs to employ numerical technique like shooting method to obtain the pressure distribution subjected to the isobaric condition at the two exits (i.e. at $x=0, l$; $p = p_{atm}$). This pressure distribution is now used to evaluate the load bearing capacity of the channel (\tilde{w}) as

$$\tilde{w}_{11} = \frac{w_{11}}{\mu u_{hs}} = \delta \int_0^1 \bar{p}_{11} d\bar{x} \quad (20)$$

For conciseness, solutions for $O(\gamma)$ and higher orders are presented in the **Appendix** section. Physically, in addition to surface charge and slip length alterations, further disturbance in the flow field comes from the addition of polymer which introduces several interactions within the flow domain thus influencing strongly the degree of deformation. This is discussed in detail in the results and discussions section.

4 Results and discussion

In this section, first we discuss the effect of two modulation parameters on the flow field and the associated load bearing capacity ($\tilde{W}/\tilde{W}_{\text{ref}}$) briefly. Here, the effect of wettability modulation (δ) can be described solely by the Navier's slip condition, which by definition is a strong function of the velocity gradient at the surface. Now, the imposition of wettability gradient creates a disturbance in the wall adjacent flow velocity which is further propagated to the next layer through viscous interaction. Now, because of inherent compliance, there is always a tendency to maintain the original channel height which in turn, induces a pressure gradient and lift force thus leading to channel deformation. Similarly, surface charge patterning (γ) has an immediate effect in the flow field within the EDL, which typically exists near the wall in microscale flows. (The thickness of EDL lies within

1-100 nm while the channel height ranges between 1 to 100 micron) The effect of electrokinetic forcing is strongly manifested as one starts increasing γ thereby inducing more lift force and load bearing capacity as a consequence.

Before presenting the results, a short discussion about the background is presented such that it can be easier to correlate from experimental perspective. Here, Deborah number (De) is a very important characteristic dimensionless number associated with the flow of viscoelastic fluids and intuitively, one can be keen to see its effect on the flow field and the associated deformation characteristics. However, instead of representing parametric variation, we have chosen to show the variations of physically realizable parameters such that it can be executed in actual experimental scenarios. Towards this, we use the definition of De ($De = \lambda \kappa u_{hs}$) which clearly shows the dependence on two parameters, i.e., fluid viscosity (μ) and fluid relaxation time (λ) which can easily be modulated by means of polymer concentration (c). Physically, this also represents the relative strength between elastic and viscous forces within the flow domain. The alteration of the rheological properties of fluid upon polymer addition is briefly presented in **Section A** of the supplementary material. Since De works as a fingerprint of departure from Newtonian behavior, any effect of viscoelasticity is noticeable only for higher values of De . Here, the elastic stresses are localized in the wall adjacent region where the EDL is present and hence, the effect of viscoelasticity is manifested only in this region and becomes diminished at the bulk where it shows almost Newtonian like behavior.

As discussed in the supplementary material, depending on polymer concentration (c), solution may experience a transition from one regime to another.⁸³⁻⁸⁸ These regimes are divided into three parts, namely, dilute, semi-dilute unentangled and semi-dilute entangled. Here we have chosen two representative examples of aqueous solution of Polyethylene Oxide (PEO) and Polyacrylamide (PAM) where different regimes are demarcated in Figs. 2 (i), (ii) with c^* and c_e being the overlap and entanglement concentrations respectively. In the dilute regime, as c is increased gradually, as reflected in the scaling relationship, fluid exhibits both viscous and elastic behavior. Here, viscosity (μ) follows a linear relationship with c while relaxation time (λ) remains constant for a dilute

solution (for a dilute solution, Zimm's relaxation time (λ_z) is typically employed which is independent of c , i.e. $\lambda \propto c^0$). Physically, this increment in μ will try to resist the disturbance caused by the two perturbation parameters δ and γ . However, as shown in insets (a),(c) of Fig. 2, this rise in viscosity is not significant, only ~ 1.4 times as c is increased up to c^* which implies that the strength of elastic force is strong enough to create a deformation of the polymer chain away from its equilibrium position. This subsequently creates a disturbance on the already perturbed flow field and induces more lift force as compared to that of Newtonian fluid. As a result, load bearing capacity (\tilde{W}) in the dilute regime is much higher with respect to Newtonian fluid (\tilde{W}_{Ref}). However, with increasing c , the enhanced viscous resistance leads to reduction in $\tilde{W}/\tilde{W}_{\text{Ref}}$, it decreases from ~ 1.6 times to ~ 1.3 times as c is approaching towards c^* and obeys the following scaling: $\tilde{W}/\tilde{W}_{\text{Ref}} \sim c^{-0.28}$ (for PEO) and $\tilde{W}/\tilde{W}_{\text{Ref}} \sim c^{-0.29}$ (for PAM) respectively.

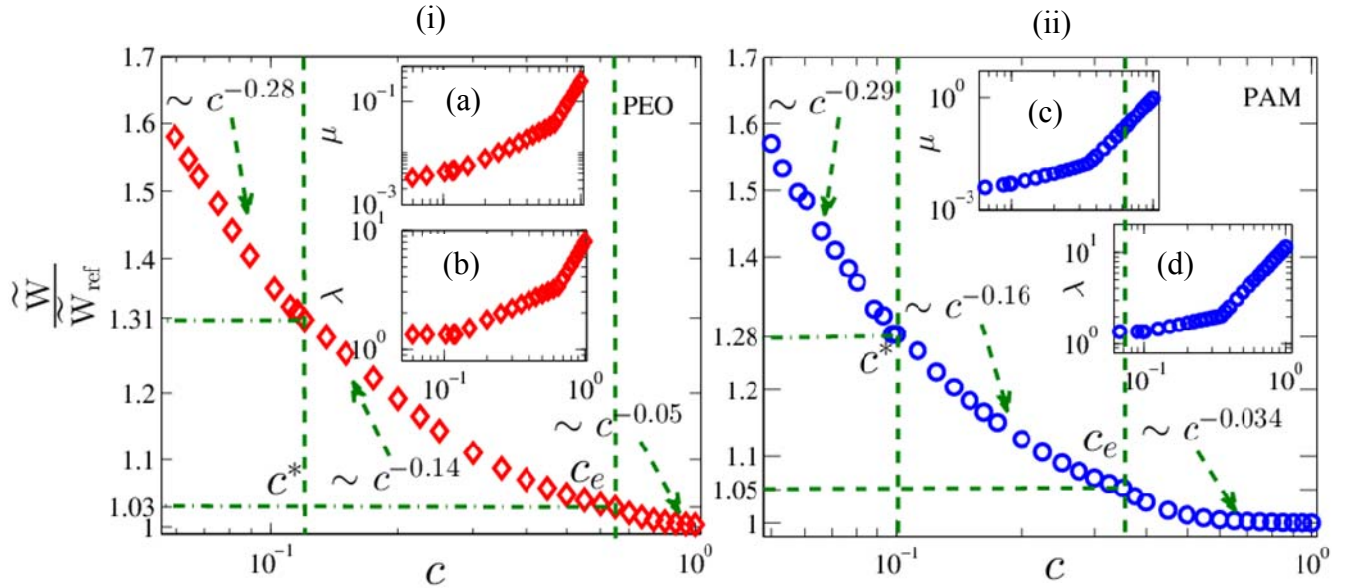


Fig. 2 Load bearing capacity ($\tilde{W}/\tilde{W}_{\text{Ref}}$) variation with increasing concentration of the aqueous polymer solution (c). (i) is for aqueous Polyethylene Oxide (PEO) solution, (ii) for aqueous Polyacrylamide (PAM) solution. Also, inset (a),(c) are the results for viscosity variation (in Pa. s.) while inset (b),(d) corresponds to relaxation time (λ) variation (in ms) with c .⁸³ c^* and c_e are the overlap and entanglement concentrations respectively (for both cases). Results are presented at $\delta = 0.3$, $\gamma = 0.3$, $\theta = 0^\circ$, $\alpha = 0^\circ$ with \tilde{W}_{Ref} being the load bearing capacity for Newtonian fluids.

When we move from dilute to semi-dilute regime, with increasing c , both λ and μ increases. For example, as shown in the insets of Fig. 2 (ii), changing c from c^* to c_e results in an increment of ~ 1.5 times for λ and ~ 3.5 times for μ in the semi-dilute regime. Physically, more λ means more time is required for the polymer chain to return from its deformed structure into its equilibrium configuration while increase in viscosity results in suppression of the disturbance in the flow and the degree of deformation of the channel is dictated by their relative strengths. Since viscous force becomes more pronounced with increasing c , it results significant reduction in $\tilde{W}/\tilde{W}_{\text{Ref}}$, from ~ 1.3 times to ~ 1.03 times in PEO (or ~ 1.05 times in PAM) as c is changed from c^* to c_e .

In the semi-dilute entangled regime, both parameters λ and μ show strong dependence with c . For example, changing c beyond c_e in PAM solution, augmentation of μ and λ are ~ 60 times and ~ 5 times respectively, i.e., μ is increased at least one order of magnitude as compared to λ . Although elastic force is strengthened significantly in this regime, any kind of disturbance in the flow caused by the deformed polymer chain is overshadowed by the strongly pronounced viscous forces thereby leading to significant reduction of $\tilde{W}/\tilde{W}_{\text{Ref}}$ beyond c_e . Increasing c beyond c_e creates a scenario when $\tilde{W}/\tilde{W}_{\text{Ref}}$ approaches unity which implies that the degree of deformation employing viscoelastic fluid (for both PEO and PAM) coincides with that of Newtonian fluid. Hence, from experimental point of view, if one actually wants to enhance the load bearing capacity of lubricated systems using viscoelastic fluids, solutions in dilute regime should be preferred over other regimes which also naturally involve only small addition of polymer.

Now we look into other aspects of rheological alteration of polymer solutions in the dilute regime. As per definition, solution can be safely assumed to be dilute when there is no topographical or hydro-dynamical interaction between the polymer chains.^{84,86,89-92} Just a small addition of polymer initiates several thermodynamic interactions within a Newtonian solvent out of which hydrodynamic interaction is a significant one in which disturbance in the flow field is caused by the polymer chain at one part with other part producing a drag force on the Newtonian solvent. This effect comes into prominence as one increases the molecular weight of the polymer (M_w). Here, intrinsic viscosity $[\mu]$ is a parameter associated with dilute solution which is utilized to determine the cross-over (or

overlap) concentration (c^*) (a short discussion about intrinsic viscosity is appended in **Section B** of the supplementary material). According to Flory's theory, c^* is the reciprocal of intrinsic viscosity $[\mu]$. Now, $[\mu]$ depends on M_w as $[\mu] = a M_w^b$ (also known as Mark-Houwink-Sakurada (MHS) equation)⁸⁴ with a and b being experimentally obtained empirical constants. Physically, more the value of M_w , lesser is the concentration required to reach the cross-over concentration. So, for higher M_w , very small concentration of polymer is strong enough to initiate interaction between the polymer chains. Additionally, the definition of Zimm's relaxation time (λ_z) tells us that λ_z is directly proportional to M_w . This aforesaid variations of λ_z and $[\mu]$ are depicted in insets (i) and (ii) of Fig. 3 with dilute aqueous solution of PEO being chosen as an example. As clear from these figures, the influence of M_w on λ_z is much stronger as compared to that on $[\mu]$ which results in significant enhancement in elastic stresses which in turn creates an amplified imbalance in pressure distribution. In the range $10^5 \leq M_w \leq 10^6$, effect of M_w on $\tilde{W}/\tilde{W}_{\text{Ref}}$ is indistinguishable while for beyond $M_w = 10^6$, $\tilde{W}/\tilde{W}_{\text{Ref}}$ is increased up to ~ 4.35 times by following the behavior: $\tilde{W}/\tilde{W}_{\text{Ref}} \propto M_w^{2.26}$.

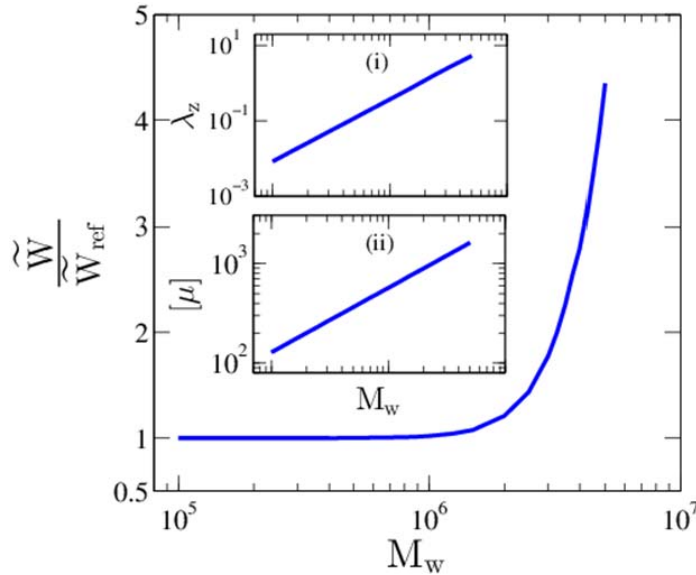


Fig. 3 The dependence of $\tilde{W}/\tilde{W}_{\text{Ref}}$ as a function of polymer molecular weight (M_w) for aqueous solution of polyethylene oxide (PEO). Inset (i) and (ii) are the variations of Zimm's relaxation time (λ_z) and intrinsic viscosity of polymer $[\mu]$ with M_w .⁸⁴

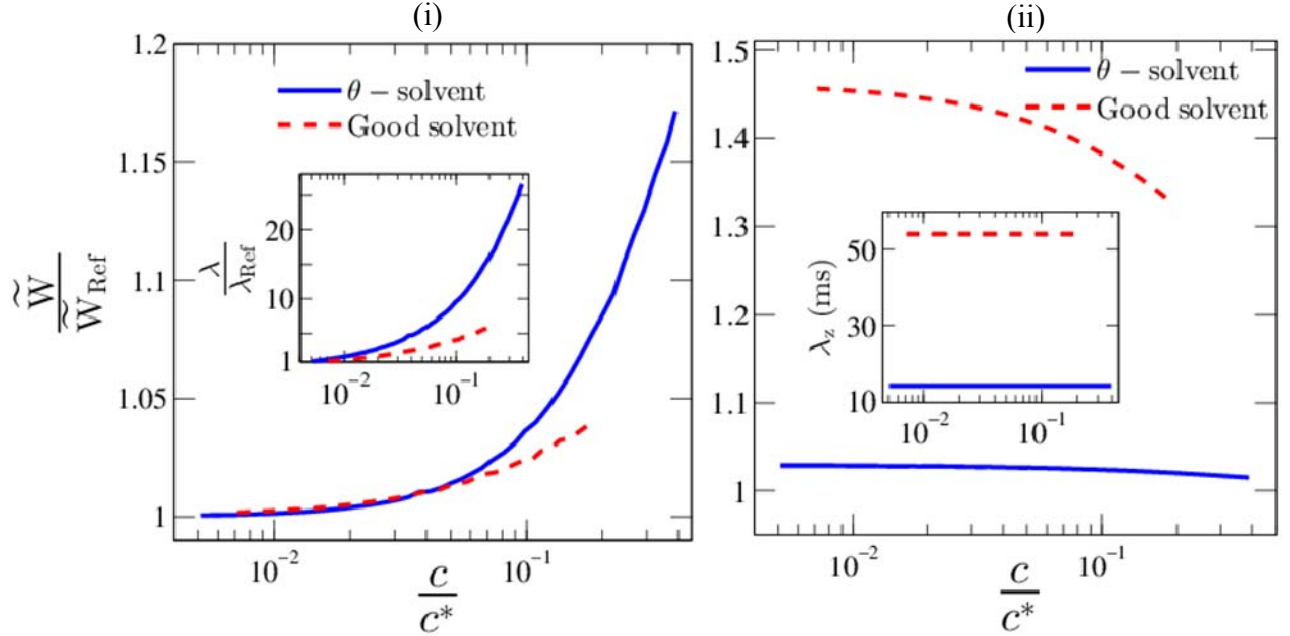


Fig. 4 The variation of $\tilde{W}/\tilde{W}_{\text{Ref}}$ with varying solvent quality. (i) incorporates results using experimentally determined fluid relaxation times, (ii) predictions according to the Zimm's relaxation time. Here, Dioctyl Phthalate (DOP) and Tricresyl Phosphate (TCP) are chosen as examples of θ -solvent and good solvents respectively while Polystyrene (PS) is chosen as the representative example of a neutral polymer ($M_w = 6.9$ MDa).⁹³ Inset of Fig. 4 (i) shows the variation of λ with c for different solvent quality while inset in Fig. (ii) shows corresponding λ_z values.

Another feature is the effect of excluded volume which becomes of critical importance when dealing with dilute polymer solution where the conformation of the polymer chain depends strongly on the quality of the Newtonian solvent.^{83,91,93} The degree of expansion of the chain is dictated by the intermolecular interaction between the polymer molecules and the solvent molecules. This is always associated with an energy of interaction which plays a pivotal role in determining whether the chain expands or contracts. If the quality of the solvent is poor enough to nullify any effect of excluded volume, then one can represent it as the fulfillment of the θ -condition thereby resulting contraction of the polymer.^{94,95} On the contrary, in good solvent the repulsion between the chains is strong enough to expand the conformation beyond the most stable configuration. This expansion makes a disturbance in the flow field which is already perturbed owing to the imposition of wettability and surface charge modulation. The combined effect of all these alterations results in an enlarged non-uniformity in the axial pressure distribution and the microchannel gets more deformed as a consequence.

In Fig. 4 (i), we have demonstrated the effect of solvent quality on the load bearing capacity ($\tilde{W}/\tilde{W}_{\text{Ref}}$). To illustrate this, we have chosen two types of solvents as examples, Dioctyl Phthalate (DOP) and Tricresyl Phosphate (TCP), which are considered as near θ -solvent (at θ -temperature 22°C) and good solvents respectively.⁹³ Microfluidic approach of relaxation time determination in recent years have shown that by monitoring the solvent quality one can get significantly different values of λ as compared to λ_z . (Regarding this, a brief discussion is added in **Section C** of the supplementary material) Mathematically, for a fixed value of c and M_w , $[\mu]$ is related as $[\mu] \propto M_w^{3\nu-1}$ which further simplifies to $M_w^{0.5}$ for θ -solvent and $M_w^{0.8}$ for good solvent respectively. Here ν is denoting the solvent quality ranging from 0.5 (θ -solvent) to 0.6 (good solvent).⁸³ Since the change of $[\mu]$ for θ -solvent is less significant as compared to good solvent, criterion for c^* is achieved at higher c thus resulting much higher λ for θ -solvent. These variation of λ with solvent quality is illustrated in inset of Fig. 4. The enhanced elastic stress is so pronounced in θ -solvent with increasing c that, although it nullifies the excluded volume effect, deformation in polymer chain leads to enhancement in $\tilde{W}/\tilde{W}_{\text{Ref}}$ of ~ 1.17 times and gets suppressed in good solvent (~ 1.04 times). This leads to the conclusion that, for achieving improved load capacity of microchannel, dilute solution consisting of θ -solvent should be deployed over good solvent.

Fig. 4 (ii) includes the predictions of $\tilde{W}/\tilde{W}_{\text{Ref}}$ using λ_z which by definition is independent of c for dilute solution while in reality, they show the dependences of $\lambda \propto c^{0.76}$ for θ -solvent and $\lambda \propto c^{0.54}$ for good solvent respectively.⁹³ As a result, use of λ_z leads to grossly erroneous predictions of $\tilde{W}/\tilde{W}_{\text{Ref}}$. As already shown in previous studies, Zimm's theory may lead of discrepancies in finding λ for good solvent which is also observed here by the opposite trends with respect to Fig. 4 (i).

Now, we focus our attention towards polyelectrolyte solutions^{85,93,96,97} which exhibit strikingly distinct behavior as compared to neutral polymer solutions. For neutral polymers, below c^* , no interaction takes place between the chains, while for polyelectrolyte solutions, strong intermolecular interaction occurs at much lower concentration than c^* which results in swelling of the chain. With increasing c , strengthened interaction between polymer chains results in increase in

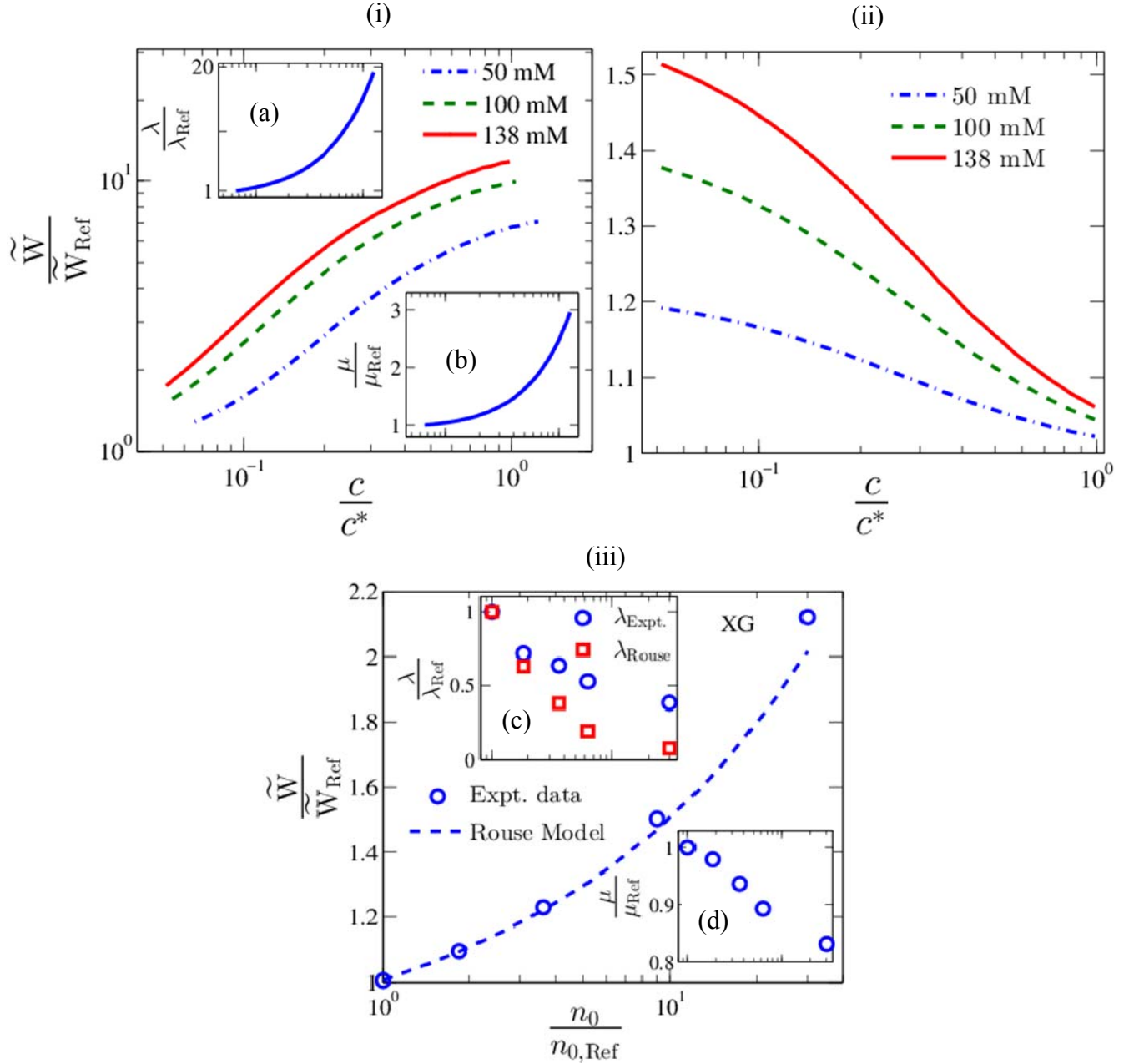


Fig. 5 (i)-(ii) The dependence of $\frac{\langle \tilde{W} \rangle}{\langle \tilde{W} \rangle_{\text{Ref}}}$ with c for different n_0 of electrolyte NaCl. (i)-(ii) corresponds results using dilute Hyaluronic acid (HA) solution ($M_w = 1.6$ MDa) in Phosphate buffered Saline (PBS) solution with (i) using expt. data for rheological parameters while (ii) uses predictions according to Zimm's theory. Inset (a) and (b) in (i) shows the variation of λ and μ with increasing c with λ_{Ref} and μ_{Ref} being evaluated at $c/c^* = 0.066$. (iii) represents results for semi-dilute aqueous Xanthan gum solution (XG) where inset (c) and (d) depict the dependence of λ and μ with n_0 . Here, $n_{0,\text{Ref}} = 0.013$ wt% is the reference n_0 of electrolyte KCl.

both fluid viscosity (μ) and relaxation time (λ) where the growth of λ is much faster as compared to μ . As clear from inset (a) and (b) of Fig. 5 (i), relative increment for μ is ~ 3 times and ~ 20 times for λ . Thus relative strength of elastic force as compared to viscous force increases. Here, non-uniformity in the flow field is already induced by virtue of two modulations and the strengthened elastic stress results strong deformation of the polymer chains. Higher the value of c , higher is the difficulty to return into its original form thereby inducing more imbalance in the pressure distribution and the deformation is significantly pronounced. As shown in Fig. 5 (i), increasing c (keeping n_0 constant) gradually up to c^* results in ~ 7 times augmentation in $\tilde{W}/\tilde{W}_{\text{Ref}}$ where the rheological properties of dilute Hyaluronic acid (HA) in Phosphate buffered Saline (PBS) solution has been chosen as a polyelectrolyte.⁹³

In absence of salt or in the low salt regime, electrostatic repulsion between the free charges of the polymer results in an expansion of the polymer conformation. As we start adding electrolyte, this interaction gets screened by the counterions thereby resulting contraction of the polymer. This alteration in the molecular conformation significantly affects the rheological properties of the fluid like viscosity, relaxation time. Subsequently, increasing n_0 from 50 mM to 138 mM (using NaCl as an electrolyte) results in $\sim 66\%$ increment of $\tilde{W}/\tilde{W}_{\text{Ref}}$, clearly seen from Fig. 5 (i).

Now, Fig. 5 (ii) shows the variation of same using theoretically estimated rheological parameters. As discussed earlier, λ dependence of polyelectrolyte solution with c is completely different as compared to neutral polymer, for which according to Zimm's theory, λ is independent of c . Since usage of Zimm's definition of λ fails to incorporate intermolecular interaction in polyelectrolyte solutions, it leads to erroneous predictions of load bearing capacity where opposite trend of $\tilde{W}/\tilde{W}_{\text{Ref}}$ variation with c is observed in Fig. 5 (ii).

This figure also incorporates the effect of rheological alteration in aqueous semi-dilute unentangled solution upon salt addition (Fig. 5 (iii)). For example, the molecular structure of Xanthan gum (XG) is governed by the presence of charged side chains as well as the free ions in the solvent. Upon salt addition, it experiences a transition in the molecular structure from extended to rod-like conformation, i.e. reduction in the hydrodynamic size takes place. This structural change affects

strongly the rheological properties of Xanthan Gum (XG) which immediately influences the associated flow field. The variation of $\tilde{W}/\tilde{W}_{\text{Ref}}$ with varying n_0 using semi-dilute XG solution is shown in Fig. 5 (iii) where $n_{0,\text{Ref}}$ is the reference electrolyte concentration of KCl, i.e., $n_{0,\text{Ref}} = 0.013$ wt % with \tilde{W}_{Ref} being the load capacity corresponding to $n_{0,\text{Ref}}$ using Newtonian fluid.⁹⁶ Owing to this alteration with increasing n_0 , the flow field is strongly affected. However, $\tilde{W}/\tilde{W}_{\text{Ref}}$ is still increasing with n_0 . with an increment of ~ 2.1 times being observed at $n_0/n_{0,\text{Ref}} \sim 30$. In this context, it is important to mention that as n_0 is increased monotonically, the thickness of electrical double layer (EDL) (λ_D) decreases and for very high n_0 , the EDL becomes so thin that the effect of electrokinetic modulation is diminished and major contribution comes from slip length modulation. As a result, despite being actual relaxation time significantly different to that predicted by Rouse model^{85,97} (a discussion about Rouse model is included in **Section D** of the supplementary material), predictions of $\tilde{W}/\tilde{W}_{\text{Ref}}$ for experimental and remains identical for lower n_0 (up to $n_0/n_{0,\text{Ref}} \sim 5$) while some under-estimation by Rouse model is observed for higher n_0 (i.e. at $n_0/n_{0,\text{Ref}} \sim 30$).

The culmination of the results and discussion section shows the respective deformations for the previously described conditions, as depicted in Fig. 6. For a fixed value of electrokinetic and hydrodynamic modulations, fixed substrate stiffness and electrolyte concentration, use of dilute polymer solution results in substantial increase in the degree of deformation (d/h) with maximum increment of ~ 66 % obtained as compared to the Newtonian fluid while for semi-dilute solution, this increment is attenuated with the maximum increment being half of that observed in dilute solution (Fig. 6 (i)). Similarly, the corresponding deformation for entangled solution is indistinguishable from that of Newtonian fluid which again supports the claim that dilute solution should be employed over other solutions. While dealing with polymer molecular weights, d/h is very less for low molecular weight solution (identical for $M_w = 10^5$ and $M_w = 10^6$) and noticeable effect can only be obtained at higher M_w . As evident from Fig. 6 (ii), changing M_w from 10^6 to 5×10^6 gives rise to ~ 5 times enhancement in the degree of deformation. Additionally, maximum increment of ~ 17.4 % is observed as one employs θ -solvent instead of good solvent. Finally, among all these cases, the effect

of electrolyte concentration is strongest for causing maximum extent of deformation which naturally results maximum load bearing capacity of the channel.

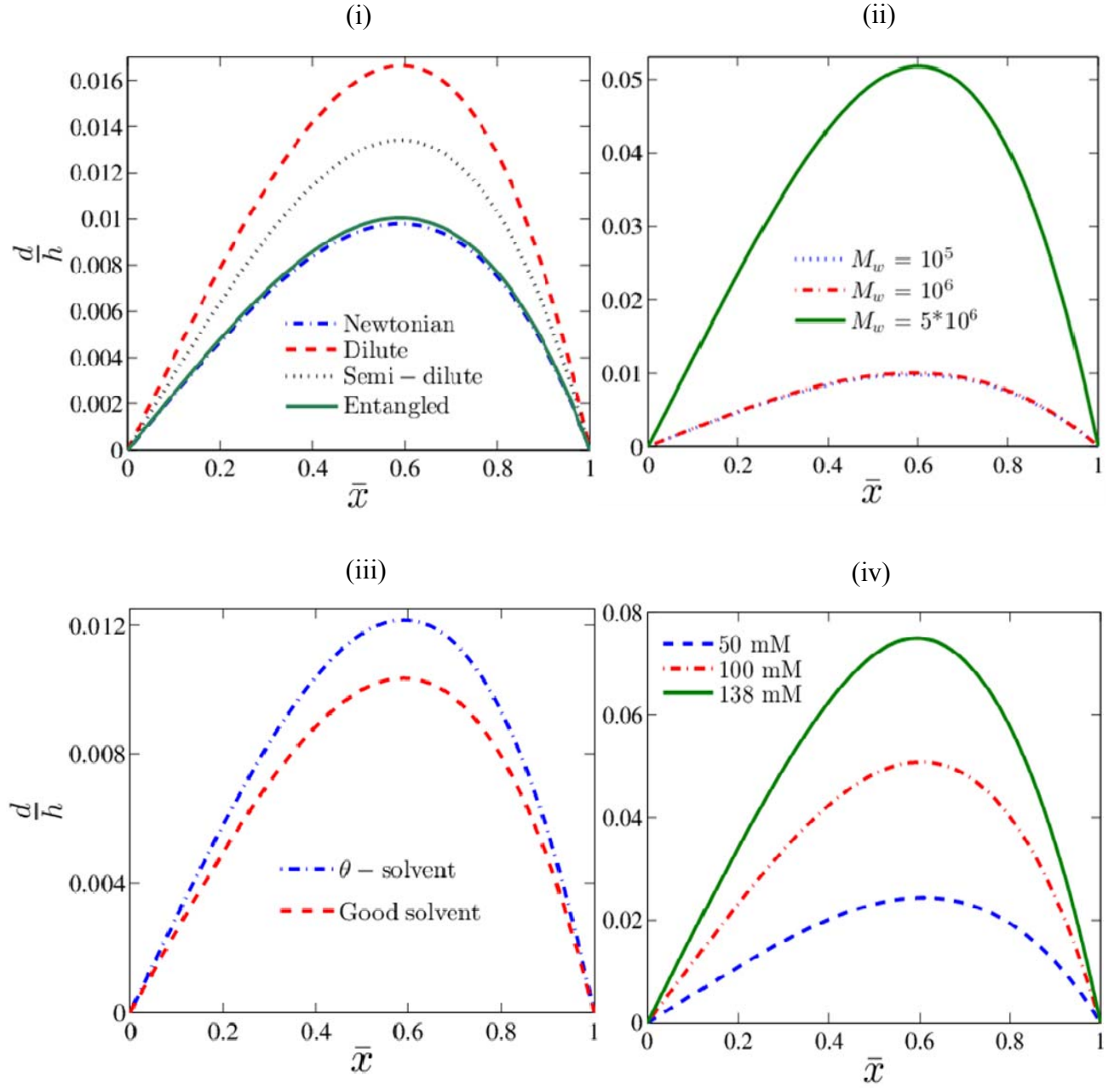


Fig. 6 Degree of deformation (d/h) with (i) varying polymer concentration (c), (ii) varying polymer molecular weight (M_w), (iii) varying solvent quality (θ -solvent or good solvent) (iv) varying electrolyte concentration (n_0).

5 Conclusions

The primary objective of the present analysis is to delineate the alteration in the deformation characteristics of a compliant microfluidic channel under the rheological premises of viscoelastic fluids, typically reminiscent of complex biological fluids. As previously reported, the coupling between interfacial hydrodynamics and electrokinetics in association with surface compliance can significantly amplify the load bearing capacity of the microchannel.⁷¹ Here, we show that further enhancement can be achieved by judiciously choosing experimentally tunable parameters. For example, using proper concentration of polymer, molecular weight, monitoring the quality of solvent, modulating electrolyte concentration in polyelectrolyte solutions it is practically possible to enhance the load bearing capacity up to one order of magnitude as compared to that of Newtonian fluid. We understand that these outcomes may construct a new paradigm in the context of improved and optimal designing of lubricated system involving biofluids thus bearing strong contemporary relevance.

Conflicts of interest

There are no conflicts to declare.

Acknowledgements

One of the authors, SM, gratefully acknowledges the help of Mr. Jayabrata Dhar (Post-doctoral researcher, Université de Rennes, CNRS, Géosciences Rennes UMR6118, Rennes, France) regarding the problem formulation part.

Appendix

Section A: Solutions for $O(\gamma)$ and higher degrees of perturbations:

The governing equations for flow field and pressure distribution for $O(\gamma)$ are shown below

$$\left. \begin{aligned} 0 &= -\frac{dp_{12}}{dx} + \frac{\partial \tau_{xy,12}}{\partial y} - \varepsilon \kappa^2 \psi_{12} E \\ \frac{\partial u_{12}}{\partial y} &= \frac{\tau_{xy,12}}{\mu} + \frac{6 \in \lambda^2}{\mu^3} \tau_{xy,0}^2 \tau_{xy,12} \end{aligned} \right\} \quad (\text{A1}) \quad \text{where}$$

$$\psi_{12} = \zeta \frac{\cosh(Qy)}{\cosh(Qh)} \cos(qx + \alpha) \quad \text{and} \quad \tau_{xy,12} = \frac{dp_{12}}{dx} y + \frac{\varepsilon \kappa^2 \zeta E \sinh(Qy)}{Q \cosh(Qh)} \cos(qx + \alpha) \quad \text{with} \quad Q = \sqrt{\kappa^2 + q^2}$$

being the patterning frequency of surface charge modulation. This results in the following velocity and pressure distributions

$$\left. \begin{aligned} \bar{u}_{12} = \frac{u_{12}}{u_{hs}} &= \frac{\bar{y}^2}{2} \frac{d\bar{p}_{12}}{d\bar{x}} - \frac{\bar{\kappa}^2 F_3(\bar{x}) \cosh(\bar{Q}\bar{y})}{\bar{Q}^2 F_5(\bar{x})} - \frac{1}{2} \frac{d\bar{p}_{12}}{d\bar{x}} \bar{h}^2 + \frac{\bar{\kappa}^2 F_3(\bar{x})}{\bar{Q}^2} \\ &+ \frac{3sDe^2}{2 \cosh^2(\bar{\kappa} F_2(\bar{x}))} \left(\frac{1}{\bar{\kappa}^2} \frac{d\bar{p}_{12}}{d\bar{x}} (\bar{\kappa} \bar{y} \sinh(2\bar{\kappa} \bar{y}) - \bar{\kappa}^2 \bar{y}^2 - \cosh^2(\bar{\kappa} \bar{y})) \right. \\ &\left. - \frac{\bar{\kappa}^2 F_3(\bar{x})}{\bar{Q} F_5(\bar{x})} \left(\nu_5 \cosh(\bar{y}/\nu_5) + \nu_6 \cosh(\bar{y}/\nu_6) - \frac{2 \cosh(\bar{Q}\bar{y})}{\bar{Q}} \right) \right) \\ &- \bar{l}_s \left(\frac{d\bar{p}_{12}}{d\bar{x}} F_2(\bar{x}) - \frac{\bar{\kappa}^2 \nu_9 F_3(\bar{x})}{\bar{Q}} + 6sDe^2 \left(\frac{d\bar{p}_{12}}{d\bar{x}} F_2(\bar{x}) \nu_7^2 - \frac{\bar{\kappa}^2 F_3(\bar{x}) \nu_7^2 \nu_9}{\bar{Q}} \right) \right) \\ &- \frac{3sDe^2}{2 \cosh^2(\bar{\kappa} F_2(\bar{x}))} \left(\frac{1}{\bar{\kappa}^2} \frac{d\bar{p}_{12}}{d\bar{x}} (\bar{\kappa} F_2(\bar{x}) \sinh(2\bar{\kappa} F_2(\bar{x})) - \bar{\kappa}^2 \bar{h}^2 - \cosh^2(\bar{\kappa} F_2(\bar{x}))) \right. \\ &\left. - \frac{\bar{\kappa}^2 F_3(\bar{x})}{\bar{Q} F_5(\bar{x})} (\nu_5 \cosh(F_2(\bar{x})/\nu_5) + \nu_6 \cosh(F_2(\bar{x})/\nu_6) - F_{11}(\bar{x})) \right) \end{aligned} \right\} \quad (\text{A2})$$

$$\text{and} \quad \nu_1 \frac{d^2 \bar{p}_{12}}{d\bar{x}^2} + \nu_2 \left(\frac{d\bar{p}_{12}}{d\bar{x}} \right)^2 + \nu_3 \frac{d\bar{p}_{12}}{d\bar{x}} + \nu_4 = 0 \quad (\text{A3})$$

Similarly for $O(\delta^2)$, the governing equations along with their solutions are as follows

$$\left. \begin{aligned} 0 &= -\frac{dp_{21}}{dx} + \frac{\partial \tau_{xy,21}}{\partial y} \\ \frac{\partial u_{21}}{\partial y} &= \frac{\tau_{xy,21}}{\mu} + \frac{6 \in \lambda^2}{\mu^3} (\tau_{xy,0}^2 \tau_{xy,21} + \tau_{xy,0} \tau_{xy,11}^2) \quad \text{where} \quad \tau_{xy,21} = \frac{dp_{21}}{dx} y \end{aligned} \right\} \quad (\text{A4})$$

$$\left. \begin{aligned}
\bar{u}_{21} = \frac{u_{21}}{u_{hs}} = \frac{\bar{y}^2}{2} G_9(\bar{x}) + \frac{3}{2} \frac{sDe^2 G_9(\bar{x})}{\bar{\kappa}^2 \cosh^2(\bar{\kappa}\bar{h})} (2\bar{\kappa}\bar{y} \sinh(\bar{\kappa}\bar{y}) \cosh(\bar{\kappa}\bar{y}) - \bar{\kappa}^2 \bar{y}^2 - \cosh^2(\bar{\kappa}\bar{y})) \\
- \frac{6sDe^2 (G_2(\bar{x}))^2}{\bar{\kappa}^4 \cosh^2(\bar{\kappa}\bar{h})} (\bar{\kappa}^2 \bar{y}^2 \cosh(\bar{\kappa}\bar{y}) - 2\bar{\kappa}\bar{y} \sinh(\bar{\kappa}\bar{y}) + 2 \cosh(\bar{\kappa}\bar{y})) \\
- \bar{l}_s \left(G_9(\bar{x}) \bar{h} + 6sDe^2 G_9(\bar{x}) \bar{h} v_7^2 - \frac{6sDe^2}{\bar{\kappa}} \bar{h}^2 v_7 (G_2(\bar{x}))^2 \right) \\
- \bar{l}_s \cos(\bar{q}\bar{x} + \bar{\theta}) \left(G_2(\bar{x}) \bar{h} + 6sDe^2 \bar{h} v_7^2 \frac{d\bar{p}_{11}}{d\bar{x}} \right) - \frac{1}{2} G_9(\bar{x}) \bar{h}^2 \\
- \frac{3}{2} \left(\frac{sDe^2}{\bar{\kappa}^2} G_9(\bar{x}) (2\bar{\kappa}\bar{h} v_7 - \bar{\kappa}^2 \bar{h}^2 \operatorname{sech}^2(\bar{\kappa}\bar{h}) - 1) \right) + \frac{6sDe^2}{\bar{\kappa}^4} (G_2(\bar{x}))^2 (\bar{\kappa}^2 \bar{h}^2 - 2\bar{\kappa}\bar{h} v_7 + 2)
\end{aligned} \right\} \quad (\text{A5})$$

and
$$\xi_1 \frac{d^2 \bar{p}_{21}}{d\bar{x}^2} + \xi_2 \left(\frac{d\bar{p}_{21}}{d\bar{x}} \right)^2 + \xi_3 \frac{d\bar{p}_{21}}{d\bar{x}} + \xi_4 = 0 \quad (\text{A6})$$

For $O(\delta\gamma)$:

$$\left. \begin{aligned}
0 = -\frac{dp_{23}}{dx} + \frac{\partial \tau_{xy,23}}{\partial y} \\
\frac{\partial u_{23}}{\partial y} = \frac{\tau_{xy,23}}{\mu} + \frac{6 \in \lambda^2}{\mu^3} (\tau_{xy,0}^2 \tau_{xy,21} + 2\tau_{xy,0} \tau_{xy,11} \tau_{xy,12}) \quad \text{where } \tau_{xy,23} = \frac{dp_{23}}{dx} y
\end{aligned} \right\} \quad (\text{A7})$$

$$\begin{aligned}
\bar{u}_{23} = \frac{u_{23}}{u_{hs}} = \frac{\bar{y}^2}{2} \frac{d\bar{p}_{23}}{d\bar{x}} + \frac{3}{2} \frac{sDe^2}{\bar{\kappa}^2 \{G_{11}(\bar{x})\}^2} \frac{d\bar{p}_{21}}{d\bar{x}} (2\bar{\kappa}\bar{y} \sinh(\bar{\kappa}\bar{y}) \cosh(\bar{\kappa}\bar{y}) - \bar{\kappa}^2 \bar{y}^2 - \cosh^2(\bar{\kappa}\bar{y})) \\
- \frac{12sDe^2}{\bar{\kappa} G_{11}(\bar{x})} \frac{d\bar{p}_{11}}{d\bar{x}} \left(\frac{1}{\bar{\kappa}^3} \frac{d\bar{p}_{12}}{d\bar{x}} (\bar{\kappa}^2 \bar{y}^2 \cosh(\bar{\kappa}\bar{y}) - 2\bar{\kappa}\bar{y} \sinh(\bar{\kappa}\bar{y}) + 2 \cosh(\bar{\kappa}\bar{y})) \right. \\
\left. - \frac{\bar{\kappa}^2 F_3(\bar{x})}{2\bar{Q} G_{10}(\bar{x})} \left(\omega_5 \bar{y} \sinh((\bar{Q} + \bar{\kappa})\bar{y}) - \cosh((\bar{Q} + \bar{\kappa})\bar{y}) \omega_5^2 \right) \right. \\
\left. - \frac{\bar{\kappa}^2 F_3(\bar{x})}{2\bar{Q} G_{10}(\bar{x})} \left(-\omega_6 \bar{y} \sinh((\bar{Q} - \bar{\kappa})\bar{y}) + \cosh((\bar{Q} - \bar{\kappa})\bar{y}) \omega_6^2 \right) \right) \\
- \bar{l}_s \left(\frac{d\bar{p}_{23}}{d\bar{x}} \bar{h} + 6sDe^2 \frac{d\bar{p}_{21}}{d\bar{x}} \bar{h} v_7^2 - \frac{12sDe^2}{\bar{\kappa}} \frac{d\bar{p}_{11}}{d\bar{x}} \left(\frac{d\bar{p}_{12}}{d\bar{x}} \bar{h}^2 v_7 - \bar{\kappa}^2 \bar{h} v_7 \frac{v_9}{\bar{Q}} F_3(\bar{x}) \right) \right) \\
- \bar{l}_s \cos(\bar{q}\bar{x} + \bar{\theta}) \left(\frac{d\bar{p}_{12}}{d\bar{x}} \bar{h} - \frac{\bar{\kappa}^2 v_9 F_3(\bar{x})}{\bar{Q}} + 6sDe^2 \left(\frac{d\bar{p}_{12}}{d\bar{x}} \bar{h} v_7^2 - \frac{\bar{\kappa}^2 v_7^2 v_9 F_3(\bar{x})}{\bar{Q}} \right) \right) \\
- \frac{1}{2} \frac{d\bar{p}_{23}}{d\bar{x}} \bar{h}^2 - \frac{3}{2} \frac{sDe^2}{\bar{\kappa}^2 \{G_{11}(\bar{x})\}^2} \frac{d\bar{p}_{21}}{d\bar{x}} (2\bar{\kappa}\bar{h} \sinh(\bar{\kappa} G_1(\bar{x})) - \bar{\kappa}^2 \bar{h}^2 - \{G_{11}(\bar{x})\}^2) \\
+ \frac{12sDe^2}{\bar{\kappa}} \frac{d\bar{p}_{11}}{d\bar{x}} \left(\frac{1}{\bar{\kappa}^3} \frac{d\bar{p}_{12}}{d\bar{x}} (\bar{\kappa}^2 \bar{h}^2 G_{11}(\bar{x}) - 2\bar{\kappa}\bar{h} v_7 + 2) - \frac{\bar{\kappa}^2 F_3(\bar{x})}{2\bar{Q} G_{10}(\bar{x}) G_{11}(\bar{x})} \left(G_1(\bar{x}) G_6(\bar{x}) \omega_5 - G_5(\bar{x}) \omega_5^2 \right) \right. \\
\left. - \frac{\bar{\kappa}^2 F_3(\bar{x})}{2\bar{Q} G_{10}(\bar{x}) G_{11}(\bar{x})} \left(-\omega_6 \bar{h} G_8(\bar{x}) + G_7(\bar{x}) \omega_6^2 \right) \right) \quad (\text{A8})
\end{aligned}$$

and

$$\omega_1 \frac{d^2 \bar{p}_{23}}{d\bar{x}^2} + \omega_2 \left(\frac{d\bar{p}_{23}}{d\bar{x}} \right)^2 + \omega_3 \frac{d\bar{p}_{23}}{d\bar{x}} + \omega_4 = 0 \quad (\text{A9})$$

Now, the total load carrying capacity of the channel is the combined consequences of all perturbations which is given by

$$\tilde{w} = \tilde{w}_{11} + \tilde{w}_{12} + \tilde{w}_{21} + \tilde{w}_{23} = \delta \int_0^1 \bar{p}_{11} d\bar{x} + \gamma \int_0^1 \bar{p}_{12} d\bar{x} + \delta^2 \int_0^1 \bar{p}_{21} d\bar{x} + \delta \gamma \int_0^1 \bar{p}_{23} d\bar{x} \quad (\text{A10})$$

The coefficients of velocity and pressure distribution for different orders of perturbations can be found in **Section E** of the supplementary material. Also, a list of symbols with their physical meanings is attached in **Section F** for ease of understanding.

References

- 1 A. J. Grodzinsky, H. Lipshitz and M. J. Glimcher, *Nature*, 1978, **275**, 448–450.
- 2 M. Abkarian, C. Lartigue and A. Viallat, *Phys. Rev. Lett.*, 2002, **88**, 4.
- 3 A. Yazdani and G. E. Karniadakis, *Soft Matter*, 2016, **12**, 4339–4351.
- 4 T. Ye, H. Shi, N. Phan-Thien, C. T. Lim and Y. Li, *Soft Matter*, 2018, **14**, 533–545.
- 5 J. M. Skotheim and L. Mahadevan, *Phys. Rev. Lett.*, 2004, **92**, 22–25.
- 6 J. M. Skotheim and L. Mahadevan, *Phys. Fluids*, 2005, **17**, 1–23.
- 7 J. S. Biggins and L. Mahadevan, *Soft Matter*, 2018, **14**, 7680–7689.
- 8 A. Martin, J. Clain, A. Buguin and F. Brochard-Wyart, *Phys. Rev. E*, 2002, **65**, 031605/1-031605/4.
- 9 S. Park and P. Dimitrakopoulos, *Soft Matter*, 2013, **9**, 8844.
- 10 H. Jing, S. Sinha and S. Das, *Soft Matter*, 2017, **13**, 554–566.
- 11 S. B. Elbaz and A. D. Gat, *J. Fluid Mech.*, 2014, **758**, 221–237.
- 12 I. C. Christov, V. Cognet, T. C. Shidhore and H. A. Stone, *J. Fluid Mech.*, 2018, **841**, 267–286.
- 13 O. Ozsun, V. Yakhot and K. L. Ekinci, *J. Fluid Mech.*, 2013, **734**, 1–12.
- 14 T. Salez and L. Mahadevan, *J. Fluid Mech.*, 2015, **779**, 181–196.
- 15 J. Urzay, S. G. Llewellyn Smith and B. J. Glover, *Phys. Fluids*, , DOI:10.1063/1.2799148.
- 16 R. I. Tanner, *Phys. Med. Biol.*, 1966, **11**, 119–127.
- 17 A. J. Szeri, S. C. Park, S. Verguet, A. Weiss and D. F. Katz, *Phys. Fluids*, , DOI:10.1063/1.2973188.
- 18 J. Beaucourt, T. Biben and C. Misbah, *Europhys. Lett.*, 2004, **67**, 676–682.
- 19 R. J. Wakelin, *Annu. Rev. Mater. Sci.*, 1974, **4**, 221–253.
- 20 M. B. Jones, G. R. Fulford, C. P. Please, D. L. S. McElwain and M. J. Collins, *Bull. Math. Biol.*, 2008, **70**, 323–343.
- 21 S. Jahn and J. Klein, *Phys. Today*, 2018, **71**, 48–54.
- 22 N. Selway and J. R. Stokes, *Annu. Rev. Food Sci. Technol.*, 2014, **5**, 373–393.
- 23 K. G. Naik, S. Chakraborty and J. Chakraborty, *Soft Matter*, 2017, **13**, 6422–6429.
- 24 P. Karan, J. Chakraborty and S. Chakraborty, *J. Indian Inst. Sci.*, 2018, **98**, 159–183.
- 25 B. S. Hardy, K. Uechi, J. Zhen and H. Pirouz Kavehpour, *Lab Chip*, 2009, **9**, 935–938.
- 26 E. Seker, D. C. Leslie, H. Haj-Hariri, J. P. Landers, M. Utz and M. R. Begley, *Lab Chip*, 2009, **9**, 2691–2697.

- 27 E. P. Kartalov, A. Scherer, S. R. Quake, C. R. Taylor and W. F. Anderson, *J. Appl. Phys.*, 2007, **101**, 64505.
- 28 P. Panda, K. P. Yuet, D. Dendukuri, T. Alan Hatton and P. S. Doyle, *New J. Phys.*, 2009, **11**, 115001.
- 29 D. Dendukuri, S. S. Gu, D. C. Pregibon, T. A. Hatton and P. S. Doyle, *Lab Chip*, 2007, **7**, 818–828.
- 30 M. Matse, P. Berg and M. Eikerling, *Phys. Rev. E*, 2018, **98**, 53101.
- 31 U. Mukherjee, J. Chakraborty and S. Chakraborty, *Soft Matter*, 2013, **9**, 1562–1569.
- 32 K. Raj, S. Bhattacharya, S. DasGupta and S. Chakraborty, *Lab Chip*, 2018, 3939–3948.
- 33 J. C. McDonald and G. M. Whitesides, *Acc. Chem. Res.*, 2002, **35**, 491–499.
- 34 J. Nase, A. Lindner and C. Creton, *Phys. Rev. Lett.*, 2008, **101**, 1–4.
- 35 M. K. Raj, S. DasGupta and S. Chakraborty, *Microfluid. Nanofluidics*, 2017, **21**, 1–12.
- 36 K. Raj M, J. Chakraborty, S. DasGupta and S. Chakraborty, *Biomicrofluidics*, 2018, **12**, 34116.
- 37 F. Del Giudice, F. Greco, P. A. Netti and P. L. Maffettone, *Biomicrofluidics*, 2016, **10**, 43501.
- 38 A. Ajdari, *Phys. Rev. Lett.*, 1995, **75**, 755.
- 39 A. Ajdari, *Phys. Rev. E*, 1996, **53**, 4996–5005.
- 40 A. Ajdari, *Phys. Rev. E*, 2000, **61**, R45-8.
- 41 H. A. Stone, A. D. Stroock and A. Ajdari, *Annu. Rev. Fluid Mech.*, 2004, **36**, 381–411.
- 42 A. D. Stroock, S. K. W. Dertinger, A. Ajdari, I. Mezić, H. A. Stone and G. M. Whitesides, *Science (80-.)*, 2002, **295**, 647–651.
- 43 S. S. Bahga, O. I. Vinogradova and M. Z. Bazant, *J. Fluid Mech.*, 2010, **644**, 245–255.
- 44 I. Glasgow, J. Batton and N. Aubry, *Lab Chip*, 2004, **4**, 558–562.
- 45 L. Dong, T. Nypelö, M. Österberg, J. Laine and M. Alava, *Langmuir*, 2010, **26**, 14563–14566.
- 46 M. Jin, X. Feng, L. Feng, T. Sun, J. Zhai, T. Li and L. Jiang, *Adv. Mater.*, 2005, **17**, 1977–1981.
- 47 X. Wu and G. Shi, *Nanotechnology*, 2005, **16**, 2056–2060.
- 48 Z. Guo, F. Zhou, J. Hao and W. Liu, *J. Am. Chem. Soc.*, 2005, **127**, 15670–15671.
- 49 M. Kogoma, H. Kasai, K. Takahashi, T. Moriwaki and S. Okazaki, *J. Phys. D. Appl. Phys.*, 1987, **20**, 147–149.
- 50 M. L. Olivares, L. Vera-Candioti and C. L. A. Berli, *Electrophoresis*, 2009, **30**, 921–929.
- 51 C. L. A. Berli and M. L. Olivares, *J. Colloid Interface Sci.*, 2008, **320**, 582–589.
- 52 C. L. A. Berli, *J. Colloid Interface Sci.*, 2010, **349**, 446–448.
- 53 T. Nguyen, Y. Xie, L. J. de Vreede, A. van den Berg and J. C. T. Eijkel, *Lab Chip*, 2013, **13**, 3210.
- 54 A. Bandopadhyay and S. Chakraborty, *Appl. Phys. Lett.*, , DOI:10.1063/1.4739429.
- 55 S. Das and S. Chakraborty, *Anal. Chim. Acta*, 2006, **559**, 15–24.
- 56 J. Boyd, J. M. Buick and S. Green, *Phys. Fluids*.
- 57 G. C. Georgiou, *J. Nonnewton. Fluid Mech.*, 2003, **109**, 93–114.
- 58 C. Zhao and C. Yang, *Biomicrofluidics*, , DOI:10.1063/1.3571278.
- 59 A. Bandopadhyay, U. Ghosh and S. Chakraborty, *J. Nonnewton. Fluid Mech.*, 2013, **202**, 1–11.
- 60 J. G. Oldroyd, *Proc. R. Soc. A Math. Phys. Eng. Sci.*, 1958, **245**, 278–297.
- 61 N. P. Thien and R. I. Tanner, *J. Nonnewton. Fluid Mech.*, 1977, **2**, 353–365.
- 62 R. I. Tanner, *Engineering Rheology*, Oxford University Press, 2002.
- 63 A. M. Afonso, M. A. Alves and F. T. Pinho, *J. Nonnewton. Fluid Mech.*, 2009, **159**, 50–63.
- 64 A. M. Afonso, M. A. Alves and F. T. Pinho, *J. Colloid Interface Sci.*, 2013, **395**, 277–286.
- 65 O. Bautista, S. Sánchez, J. C. Arcos and F. Méndez, *J. Fluid Mech.*, 2013, **722**, 496–532.

- 66 S. Mukherjee, P. Goswami, J. Dhar, S. Dasgupta and S. Chakraborty, *Phys. Fluids*, 2017, **29**, 72002.
- 67 M. Heil and A. L. Hazel, *Annu. Rev. Fluid Mech.*, 2011, **43**, 141–62.
- 68 J. B. Grotberg and O. E. Jensen, *Annu. Rev. Fluid Mech.*, 2004, **36**, 121–47.
- 69 U. Ghosh and S. Chakraborty, *Phys. Rev. E*, 2012, **85**, 1–13.
- 70 U. Ghosh and S. Chakraborty, *Phys. Rev. E*, 2013, **88**, 52–58.
- 71 S. Mukherjee, J. Dhar, S. DasGupta and S. Chakraborty, *arXiv Prepr. arXiv1811.12005*.
- 72 A. Steinberger, C. Cottin-Bizonne, P. Kleimann and E. Charlaix, *Phys. Rev. Lett.*, 2008, **100**, 5–8.
- 73 J. Chakraborty and S. Chakraborty, *Phys. Fluids*, , DOI:10.1063/1.3624615.
- 74 J H Masliyah and S Bhattacharjee, *Electrokinetic and Colloid Transport Phenomena*, Wiley-Interscience, 2006.
- 75 S. Das, T. Das and S. Chakraborty, *Sensors Actuators B Chem.*, 2006, **114**, 957–963.
- 76 R. F. Probstein, *Physicochemical hydrodynamics: an introduction*, Wiley, New York, 2nd edn., 1994.
- 77 S. Das, T. Das and S. Chakraborty, *Microfluid. Nanofluidics*, 2006, **2**, 37–49.
- 78 R. J. Hunter, *Zeta Potential in Colloid Science*, Academic Press, London, 1981.
- 79 S. Das and S. Chakraborty, *Langmuir*, 2010, **26**, 11589–11596.
- 80 S. S. Das, S. Kar, T. Anwar, P. Saha and S. Chakraborty, *Lab Chip*, 2018, **18**, 1560–1568.
- 81 A. Ajdari, *Phys. Rev. Lett.*, 1995, **75**, 755–758.
- 82 S. Mukherjee, J. Dhar, S. DasGupta and S. Chakraborty, *Proc. R. Soc. A Math. Phys. Eng. Sci.*, 2019, **475**, 20180522.
- 83 F. Del Giudice, G. D’Avino, F. Greco, I. De Santo, P. A. Netti and P. L. Maffettone, *Lab Chip*, 2016, **16**, 1088–1088.
- 84 V. Tiratmadja, G. H. McKinley and J. J. Cooper-White, *Phys. Fluids*, 2006, **18**, 43101.
- 85 A. V. Dobrynin, R. H. Colby and M. Rubinstein, *Macromolecules*, 1995, **28**, 1859–1871.
- 86 C. Clasen, J. P. Plog, W.-M. Kulicke, M. Owens, C. Macosko, L. E. Scriven, M. Verani and G. H. McKinley, *J. Rheol. (N. Y. N. Y.)*, 2006, **50**, 849–881.
- 87 L. E. Rodd, J. J. Cooper-White, D. V. Boger and G. H. McKinley, *J. Nonnewton. Fluid Mech.*, 2007, **143**, 170–191.
- 88 S. Mukherjee, S. S. Das, J. Dhar, S. Chakraborty and S. DasGupta, *Langmuir*, 2017, **33**, 12046–12055.
- 89 S. L. Anna and G. H. McKinley, *J. Rheol. (N. Y. N. Y.)*, 2001, **45**, 115–138.
- 90 G. H. McKinley and A. Tripathi, *J. Rheol. (N. Y. N. Y.)*, 2000, **44**, 653–670.
- 91 P. J. Flory, *Principles of Polymer Chemistry*, Cornell University Press, Ithaca, New York, 1953.
- 92 R. P. Mun, J. A. Byars and D. V. Boger, *J. Nonnewton. Fluid Mech.*, 1998, **74**, 285–297.
- 93 F. Del Giudice, S. J. Haward and A. Q. Shen, *J. Rheol. (N. Y. N. Y.)*, 2017, **61**, 327–337.
- 94 R G Larson, *The structure and rheology of complex fluids*, Oxford University Press, New York, 1999.
- 95 R. G. Larson, *J. Rheol. (N. Y. N. Y.)*, 2005, **49**, 1–70.
- 96 L. B. Smolka and A. Belmonte, *J. Nonnewton. Fluid Mech.*, 2006, **137**, 103–109.
- 97 E. Turkoz, A. Perazzo, C. B. Arnold and H. A. Stone, *Appl. Phys. Lett.*